A 768-Channel CMOS Microelectrode Array With Angle Sensitive Pixels for Neuronal Recording

Ben Johnson, *Student Member, IEEE*, Shane T. Peace, Albert Wang, *Student Member, IEEE*, Thomas A. Cleland, and Alyosha Molnar, *Member, IEEE*

***Abstract*— This paper presents a CMOS sensor array with a 768 low-noise recording sites for neural recording with 2048 intercalated angle-sensitive pixels for optical read-out. The array is highly scalable because of electrode-level digitization with serial data stream-out. The front-end amplifiers use chopping to reduce flicker noise and achieve an input-referred noise of 4.1μV_{rms} over a 3.6 kHz bandwidth while occupying an area of only 800μm^2. Digitization is performed using a distributed ramp ADC that samples every sensor site at 10 kHz. The electrodes have a 50μm pitch and are plated with platinum to increase the interface capacitance and ensure biocompatibility. The sensor array is used to refocus a lenless image and to record neural spiking and local field potentials from a mouse olfactory bulb slice.**

***Index Terms*— Action potential, angle-sensitive pixel (ASP), CMOS sensors, local field potential, low-noise amplifiers, microelectrode array (MEA), microelectrodes, neural interface.**

I. Introduction

HOW networks of neurons work together to perform complex tasks and propagate information is an active area of research. To effectively study neural ensembles, neurophysiologists employ microelectrode arrays (MEA) to simultaneously acquire electric field activity across relatively large areas of tissue. The advantages of increasing the number of recording electrodes include: 1) the possibility for a greater number of single cell recordings and 2) spatially broad analysis of local field potentials (LFPs) that can provide insights into how and why neuronal ensembles synchronize their activity. MEA data are an invaluable resources for computational neuroscience and for the study of biological learning, acute and chronic drug effects, and physiological disorders.

Conventional planar MEAs are noninvasive and function by recording electrical extracellular activity with metal electrodes (Figure 1). Signals detected at the electrode interface are amplified, passed through a low-pass filter, and then digitized. MEAs are well suited for extended *in vitro* studies using either tissue preparations, such as retinas or brain slices [1], or neuronal cell cultures [2]. Most commercially available MEAs are fabricated on passive, patterned substrates which use off-substrate amplifiers. While these MEAs typically have between 60-256 electrodes, passive routing limits the electrode scalability. CMOS MEAs can achieve a higher spatial resolution and a large effective recording area by multiplexing channels onto fewer wires. Furthermore, they can include additional modalities, such as optical recording [1], electrical stimulation [2], or temperature sensors [3].

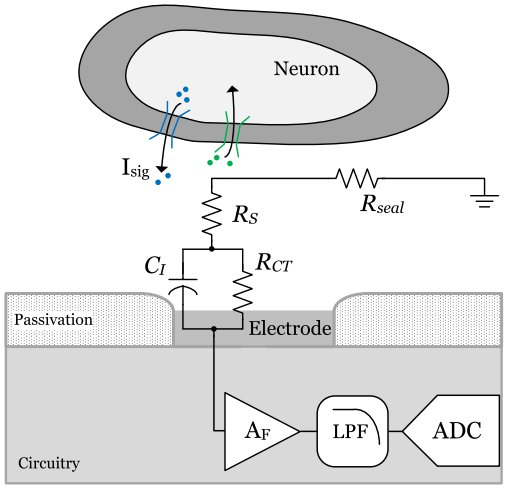

Fig. 1. Concept of planar MEA recording.

Another effective way to study neural networks with MEAs is in conjunction with optical stimulation. In visual neuroscience, computer-generated patterns of light can be used to stimulate retinal photoreceptors while electrically recording activity from the ganglion cells, the retinal output. Likewise, optogenetics allows researchers to create light-sensitive cells in other biological systems to understand the way they process information. For example, neuronal cells expressing the light-reactive protein channelrhodopsin-2 can be excited optically, circumventing the need for either electrical stimulation which creates large recording artifacts, or chemical stimulation which is nonspecific [4]. Optical stimulation can be spatially and temporally precise, cell-specific, and contact-free. Therefore, optical stimulation allows researchers to control the inputs of a neural system while an MEA allows them to record multiple intermediate and output nodes of the network.

Passive MEAs are often built on transparent substrates allowing for visual correlation of electrode location, tissue,

Manuscript received January 11, 2013; revised May 10, 2013; accepted May 21, 2013. Date of publication June 7, 2013; date of current version July 30, 2013. This was supported in part by MOSIS forChip fabrication. The associate editor coordinating the review of this paper and approving it for publication was Prof. Aime Lay-Ekuakille.

B. Johnson, A. Wang, and A. Molnar are with the School of Electrical and Computer Engineering, Cornell University, Ithaca, NY 14853 USA (e-mail: bcj25@cornell.edu; aw383@cornell.edu; molnar@ece.cornell.edu).

S. T. Peace is with the Department of Neurobiology and Behavior, Cornell University, Ithaca, NY 14853 USA (e-mail: stp33@cornell.edu).

T. A. Cleland is with the Department of Psychology, Cornell University, Ithaca, NY 14853 USA (e-mail: thomas.cleland@cornell.edu).

Color versions of one or more of the figures in this paper are available online at http://ieeexplore.ieee.org.

Digital Object Identifier 10.1109/JSEN.2013.2266894

and stimulus. Active MEAs on silicon substrates are opaque and severely limit this capability. Furthermore, CMOS MEAs can still suffer from some of the same scalability limitations of passive MEAs. State-of-the-art CMOS arrays typically tradeoff between electrode density, noise performance, and sampling rate. Therefore, the aim of this work is provide researchers with an MEA that overcomes the limitations of both traditional passive and active MEAs for slice research. The presented MEA has a high spatial resolution, a large recording area, and integrated angle-sensitive pixels (ASP [5]) to correlate optical stimuli with recorded activity. Additionally, the sensor array requires little post-CMOS processing for biocompatibility and can record from all sensors simultaneously.

This paper is organized as follows. Section II discusses the characteristics of MEA recordings as motivation for the design of the CMOS array and other state-of-the-art CMOS arrays. Section III details the system design and packaging of the sensor array. Section IV presents test results of the fabricated array and neural data acquired from a mouse olfactory bulb slice.

II. Neural Signals from MEA Recordings

A. Methods

The design was dictated by the characteristics of extracellular biopotentials recorded from olfactory bulb slices. A commercially available MEA (MEA60-Up-System, MCS GmbH) with 60 TiN electrodes was used to record extracellular fields. The electrodes had a diameter of 30μm and a pitch of 200μm. Slices were horizontally taken with a vibrating microtome with a nominal thickness of 300μm. During recording, slices were perfused with artificial cerebrospinal fluid (aCSF) containing (in mM) 125 NaCl, 25 $NaHCO_3$, 1.25 NaH_2PO_4, 25 glucose, 3 KCl, 1 $MgCl_2$. The solution was heated to 34 $^{\circ}$C using an in-line heater and oxygenated with carbogen (95% O_2, 5% CO_2). Slices were held down by a chrome harp with nylon netting.

B. Extracellular Biopotentials

According to the literature, discernible extracellular biopotentials typically range in amplitude from 10μV to about 5mV, with power in the 10-200Hz band for LFPs and 200Hz-5kHz band for action potentials [6]. Figure 2 shows the measured power spectrum of endogenous slice activity with several electrodes (n = 13). The measured spectrum was calculated by 1) averaging power spectra from a 50s long single electrode recording with 1s epochs, then 2) averaging that power spectrum with n other electrodes. The power spectrum reflects contributions from both LFP and action potentials. The LFP power peaks around 45Hz, which corresponds to the gamma band in slice (30-70Hz [7]). Gamma oscillations are ubiquitous in the brain and are indicators of synchronous cellular activity. While gamma oscillations can occur endogenously, they can also be induced chemically with glutamate receptor agonists. A spectrogram of an induced gamma oscillation is shown in Figure 3. Oscillations were also induced by optical stimuluation of slices from transgenic mice expressing channelrhodopsin-2 in the olfactory sensory neuron axons. To utilize the temporal and spatial precision of optical stimuli,

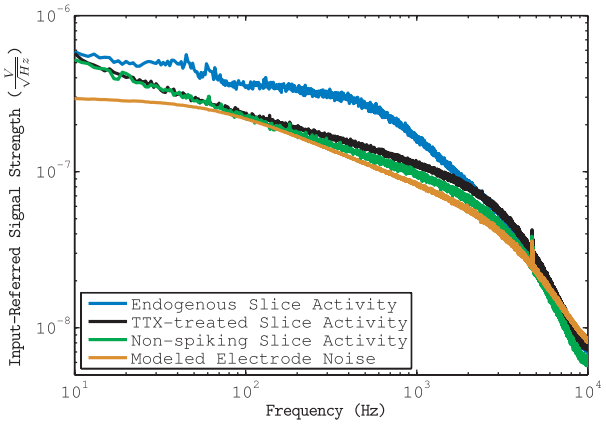

Fig. 2. Power spectra from MEA slice recordings.

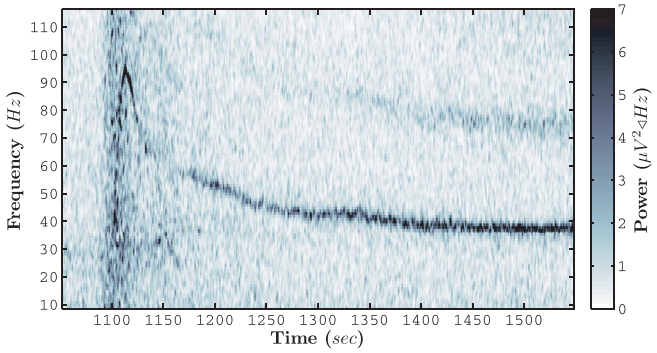

Fig. 3. A spectrogram of an induced gamma oscillation.

the proposed MEA uses photopixels to correlate light stimuli with recorded electrical activity.

Neural acquisition systems for *in vivo* recording deal with large voltage offsets from LFP, and often separate the LFP and spike bands to alleviate the dynamic range requirement of the ADC [8]. However, in this experiment the largest recorded biopotentials were on the order of 200μV_{pp}. Furthermore, the frequency content of LFP and spiking can overlap. The resultant spectral contamination means that traditional low-pass filtering methods to remove spike contributions from the LFP band may give rise to unwanted spurious correlations, problematic when studying the causal relationship between LFP and spiking. Spike removal algorithms have been shown to effectively remove spike contributions from the LFP band, assuming the recorded signal is wideband [9], [10]. Thus, the proposed MEA does not separate the LFP and spike bands on chip since more sophisticated filtering is required.

C. Background Noise Level

Recording neural signals requires low-noise instrumentation. To understand the background noise level associated with recording from slice, a sodium channel blocker, tetrodotoxin (TTX), was applied during the recordings (n = 13). This yields an estimate of the recording noise level because the spiking and oscillations have been blocked. An additional background level was obtained by averaging spectra recorded from electrodes covered by slice tissue without discernible

spikes or oscillations (n = 9). The total integrated noises were 7.2μV$_{rms}$ and 6.5μV$_{rms}$, respectively. With microelectrodes, the dominant noise source in extracellular recording typically arises from the electrode-electrolyte interface, not the recording circuitry which is often well controlled [11]. Using methods presented in [12] and [13] for the circuit model in Figure 1, we estimated the charge transfer resistance (R$_{CT}$) of the interface to be 4.7MΩ, the parallel interface capacitance (C$_I$) to be 495pF, and the spreading resistance (R$_S$) to be 12kΩ. Neglecting the Warburg impedance, the estimated noise from the interface was 4.9μV$_{rms}$. The recording circuitry had little effect on the overall noise level (2.6μV$_{rms}$), which was measured by shorting the input of the recording amplifier to ground (n = 3). In terms of frontend amplifier design, circuit noise levels much below 2.4μV$_{rms}$ contribute little to the overall noise level and are likely overdesigned, consuming unnecessary power or area. Circuit noise above 5.3μV$_{rms}$, however, is likely to be the dominant noise source for electrodes with similar geometry.

D. Spatial Spread

Measured persistent epochs (> 5 min) of gamma oscillations (30-70Hz) spanned over 600μm laterally while spiking activity from individual cells typically spread less than 100μm. This is comparable to measurements from hippocampal slices [14] and modeled results for synchronous network activity [15]. The spatial reach of gamma oscillations was determined by finding the coherence between the electrode with the highest gamma power and all other electrodes, where the coherence magnitude between two electrode recordings in the frequency domain is given by:

$$C_{xy}(\omega) = \frac{\left|\langle P_{xy}(\omega)\rangle_n\right|^2}{\langle P_{xx}(\omega)\rangle_n \cdot \langle P_{yy}(\omega)\rangle_n}. \quad (1)$$

P$_{xx}$ and P$_{yy}$ are autocorrelations and P$_{xy}$ represents the cross-correlation between the two electrodes. Note that coherence for every 1Hz frequency bin was calculated over n epochs of 1s, where n = 150. Figure 4 shows an example spatial coherence profile. In theory, adjacent electrodes exhibit no coherence in the absence of synchronous activity (μ_0 = 0) while oscillatory activity spanning multiple electrodes will be highly correlated. The variance of coherence was calculated using 58 electrodes and 20 frequency bins (21-40Hz) for a total of 1160 measures of coherence. Based on the spatial expanse of LFP, a useful planar MEA should have an active area larger than 1mm on a side to accommodate large synchronous oscillations from an entire slice and have an electrode pitch of less than 100μm to fully sample extracellular action potentials.

E. Design Requirements

Table I provides a summary of the design requirements for the CMOS sensor array derived from experimental MEA recordings. While previous work has achieved subcellular electrode pitch (<10μm) and low-noise amplification (2.4μV_{rms}), the array record from a static selection of 126 electrodes simultaneously [2]. In principle, these sites can be multiplexed faster than the bandwidth of the neural signals, allowing multiple sites to be measured each sample cycle. The difficulty with high-speed multiplexing before amplification is that noise from the interface is not filtered and is therefore aliased into relevant signal bands. Other work has used electrode-level amplification to increase the number of recording channels. [16] provides pixel-level amplification with 4,096 small pitch electrodes (42μm) but sacrifices noise performance (11μV_{rms}). Another high-density array [17] has an even finer sensor pitch (7.8μm) and more sensors (16,384), but with a much higher noise level (70μV_{rms}). Therefore the primary design challenge of CMOS MEAs is designing a low-noise amplifier with a very small area and with a scalable data read-out.

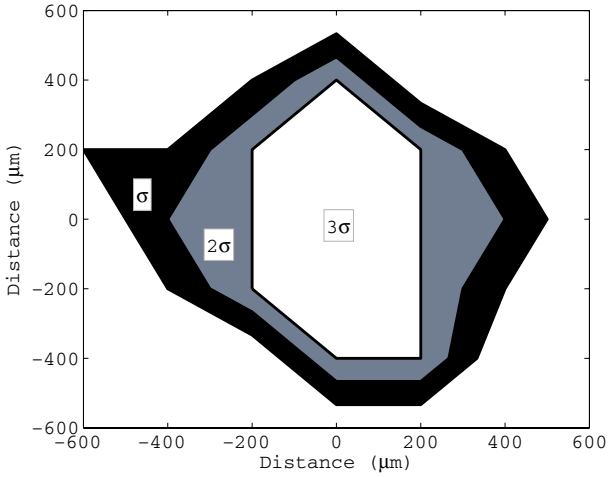

Fig. 4. Spatial coherence profile of a 33Hz olfactory bulb slice gamma oscillation (μ_0 = 0, σ = 0.067). The origin represents the location of the electrode with the highest power in the gamma band.

TABLE I
DESIGN REQUIREMENTS OF THE CMOS SENSOR ARRAY

Specification	
Signal Bandwidth	10Hz - 3kHz
Sampling Rate	10kHz
Circuit Noise	2.4μV_{rms} - 5.3μV_{rms}
Dynamic Range	>30dB
Electrode Pitch	<100μm
Spatial Extent	>600μm

III. SYSTEM DESIGN

A. System Description

The hybrid sensor array consists of 768 metal electrodes with local amplification and digitization and 2,048 photopixels. The MEA was fabricated in a standard 130nm CMOS process with an active area of 1.6mm by 1.6mm (Figure 5). An input clock (F_{in} = 40MHz) feeds a 12-bit counter in the digital core which then generates the control signals and clocks for the rest of the chip. Each sensor site is sampled at a rate of 10kHz as determined by the MSB of the counter, which is the main clock rate divided by 2^{12}. Figure 6 shows the timing diagram of the array. Sensor sampling is interleaved so that data can be output continuously at a rate equal to the main clock. There are four data output channels, each of which is

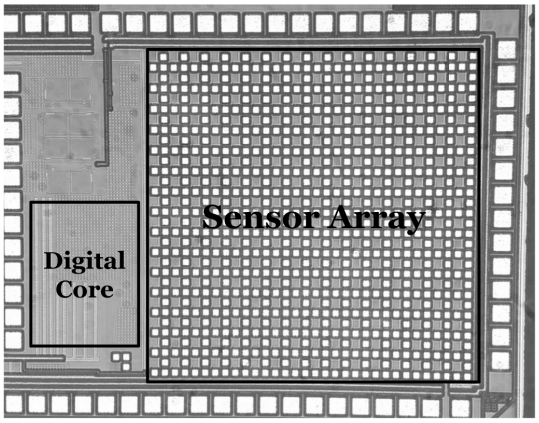

Fig. 5. Die photograph of the sensory array.

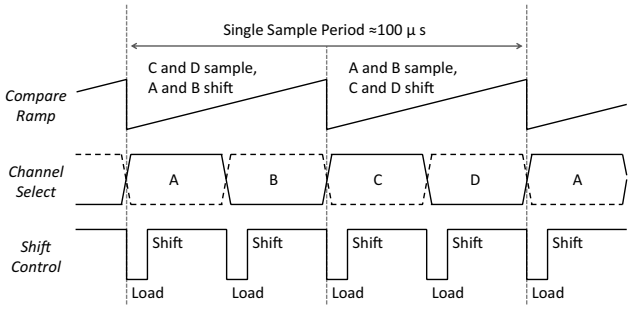

Fig. 6. Timing diagram of control signals. Half of the sensors are sampled concurrently while the other half shifts data to the output. *Channel Select* controls the subset of sensors that are shifting data and *Shift Control* facilitates the loading and shifting of the global shift registers.

fed by its own 640-bit shift register. Half of the sensors are sampled simultaneously while the other half of the sensors load and then shift data off the chip. A global 20kHz ramp signal is used as an ADC reference voltage at every sensor. The ramp is generated by a PFET current DAC controlled by the counter with a resistive load to translate the output current into a voltage. Since control signals are generated globally and the outputs are digitized, the design is highly scalable. The limiting factor of this design was the available die area.

B. Four-Sensor Subunit

Figure 7 shows the four-sensor subunit. Each subunit is comprised of three recording electrodes (**A**, **B**, **C**) and a set of 8 ASPs (**D**). Each site is allocated an area of 50μm by 45μm with an additional 50μm by 5μm of each sensor site used as part of the global shift register, which streams out the locally stored data.

The backend for the recording electrodes and the ASPs are identical. The comparator digitizes the analog signal from the sensor by comparing it to the global ramp signal. Each step of the ramp corresponds to a 10-bit value generated by the counter in the digital core. When the ramp signal is larger than the amplified signal, the comparator clocks the latch, storing the 10-bit number locally, and then shuts down to conserve power and reduce switching noise until the next sampling cycle.

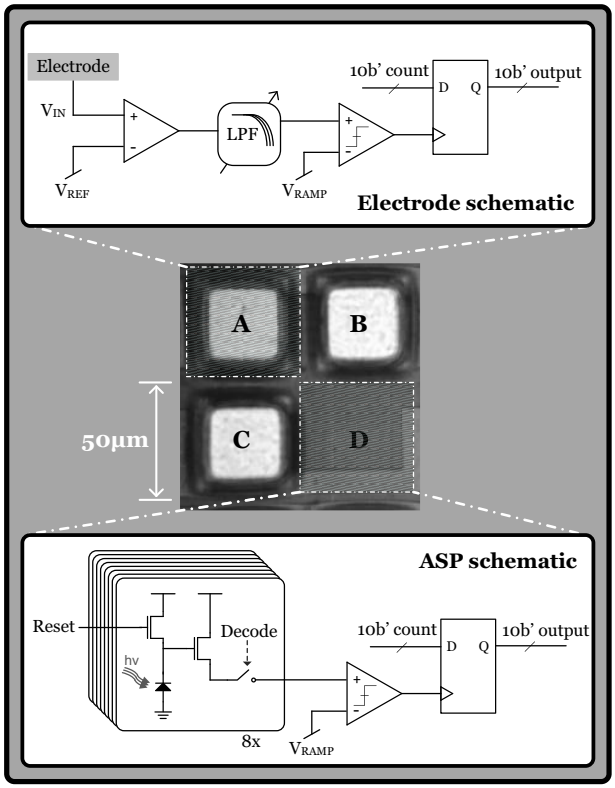

Fig. 7. Photo and architecture of four-sensor subunit. Each subunit is comprised of 3 recording electrodes (**A**, **B**, **C**) and a set of 8 ASPs (**D**).

C. Electrode Circuitry Design

Each recording electrode site contains an amplifier, a switched-capacitor low-pass filter, a comparator, and a 10-bit latch as shown in Figure 7. The metal electrode interface is defined by a passivation opening over the top metal and is formed during the standard CMOS fabrication process. V_{REF} is the applied reference potential of the electrolyte bath and is common to all the amplifiers of the array. Figure 8 shows a schematic of the folded cascode front-end amplifier. Traditional neural amplifiers use large input transistors to reduce flicker noise and large capacitors (20pF) to block electrochemical offsets [6]. To reduce area in this design, the front-end amplifier uses chopping modulation to reduce the flicker noise of the amplifier and bias the input transistors. In simulation, the total input-referred noise voltage of the amplifier over a 10kHz bandwidth is reduced by a factor of 6.6 when chopping modulation is used. The size of the input transistors are small to maintain a high input impedance ($>$20MΩ at 1.25MHz). To achieve the same performance without chopping modulation, the input transistor area would need to be increased by a factor of 43.

Low-pass filtering is needed before sampling in order to prevent aliasing of high-frequency noise from the tissue, electrode-electrolyte interface, and the amplifier. Rather than using a large load capacitor to pull the amplifier output pole to below half the sampling frequency, a much smaller MOS capacitor (C_1) was used to prevent aliasing of high-frequency chopping artifacts, followed by a switched-capacitor low-pass

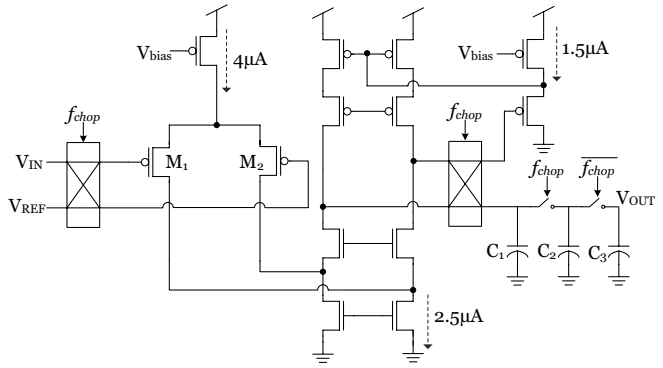

Fig. 8. Schematic of the front-end amplifier with a switched-capacitor filter.

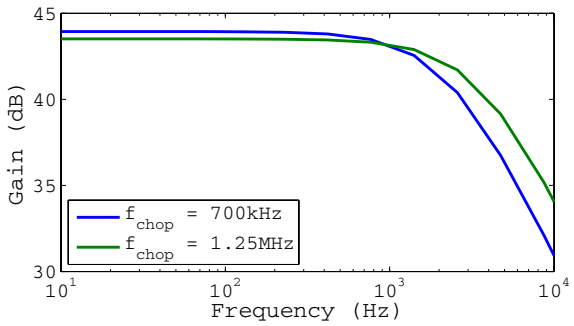

Fig. 9. Measured transfer function of the front-end amplifier with two different chopping frequencies.

filter ($\omega_L = f_{chop}C_2/C_3$). This significantly decreases the required area to get the desired pole without lowering the amplifier current, which would increase thermal noise. Furthermore, the chopping frequency controls the low-pass frequency corner. Note that the chopping frequency is controlled directly by the main clock so that the comparator always samples with the same phase. Another advantage of switched-capacitor filters is that they are relatively process invariant since their corner is set by the switching frequency and a ratio of two nearby capacitors. The amplifier and low-pass filter occupy an area of $800\mu m^2$, about 25 times smaller than neural amplifiers in MEAs with similar performance [18].

D. Angle-Sensitive Pixel Design

In place of a front-end amplifier, one-quarter of the sensor sites (**D** from Figure 7) contain eight distinct ASPs. ASPs, first introduced in [19], are devices which are sensitive to the angle of incident light and have been used to localize multiple fluorescent sources in 3D space [5] and perform post-capture computational refocus of visual scenes [20]. ASPs were implemented rather than standard photopixels because they can provide a more complete description of the light field. This is useful for understanding the scattering of stimulus light in tissue or localizing external electrodes with respect to the array. In general, ASPs use two CMOS metal gratings over a photodiode where the pitch and height between the gratings define the angular selectivity. The lower grating is used to block or pass the periodic intensity pattern generated by light striking the top grating as a function of its lateral offset. In this design, the ASPs employ two local, stacked diffraction gratings on CMOS metal layers 5 and 3 directly over a p-implant/n-well photodiode. At each sensor site there are two orientations of top diffraction grating (vertical and horizontal), and four types of bottom grating offset relative to the top grating ($\alpha = 0$, $\frac{\pi}{2}$, π, or $\frac{3\pi}{2}$), for a total of eight ASP variants. α defines the angle of peak photodiode response. Since the sampling rate needed for an ASP is much lower than an electrode, only one of the eight ASP subtypes are digitized each time for an effective sampling rate of 1.25kHz.

E. Packaging

A major difficulty with using CMOS sensors is ensuring biocompatibility and protecting wirebonds from the electrolyte solution. Most post-CMOS packaging techniques use lithographically defined epoxy or patterned PDMS to encapsulate wirebonds [21]. To simplify post-processing, epoxy was applied under a light microscope without a mask and used to encapsulate the wirebonds and define a well around the active area. The top metal of this process is aluminum, which corrodes easily in saline [22] and is also cytotoxic [23]. To prevent the electrodes from corroding, the electrodes were electroplated with platinum. Platinum is nontoxic and also decreases electrode impedance. Electroplating was performed by filling the well with a platinizing solution (chloroplatinic acid, lead acetate, hydrochloric acid). 1.5V was applied to a platinum counter-electrode to pull current through the electrodes.

IV. Experimental Results

A. System Characterization

Figure 9 shows the measured transfer function of the front-end amplifier with two different chopping frequencies. The amplifier consumed a total of $6\mu A$ from a 1.5V supply. The amplifier's bandwidth and midband gain changed from 3.6kHz and 43.5dB with a 1.25MHz chopping frequency to 2.3kHz and 43.9dB with a 700kHz chopping frequency. The total measured input-referred noise was $4.1\mu V_{rms}$ over the 3.6kHz bandwidth, corresponding to a NEF of 6.5 [24]. The ramp ADC achieved an ENOB of 8.7 bits with a $512mV_{pp}$ ramp, which corresponds to a resolution of $7.9\mu V$ at the input ($f_s = 10$kHz, $f_{in} = 100$Hz). The total power consumption of the sensor core was about 13.3mW, with 55% of the power consumed by the frontend amplifiers.

Figure 10**A** shows the normalized response of four ASP subtypes to changes in incident angle. The light was generated by a 470nm LED which was kept at a fixed distance and rotated by a micromanipulator around the sensor array. Note that the output of an ASP is a function of both intensity and incident angle, which can result in ambiguity between a bright source at a blocked angle or a dim source at a passed angle. This ambiguity is resolved by taking the difference between complementary ASPs, as shown in Figure 10**B**. The sum of the complementary ASPs encodes the intensity of the incident light (Figure 10**C**).

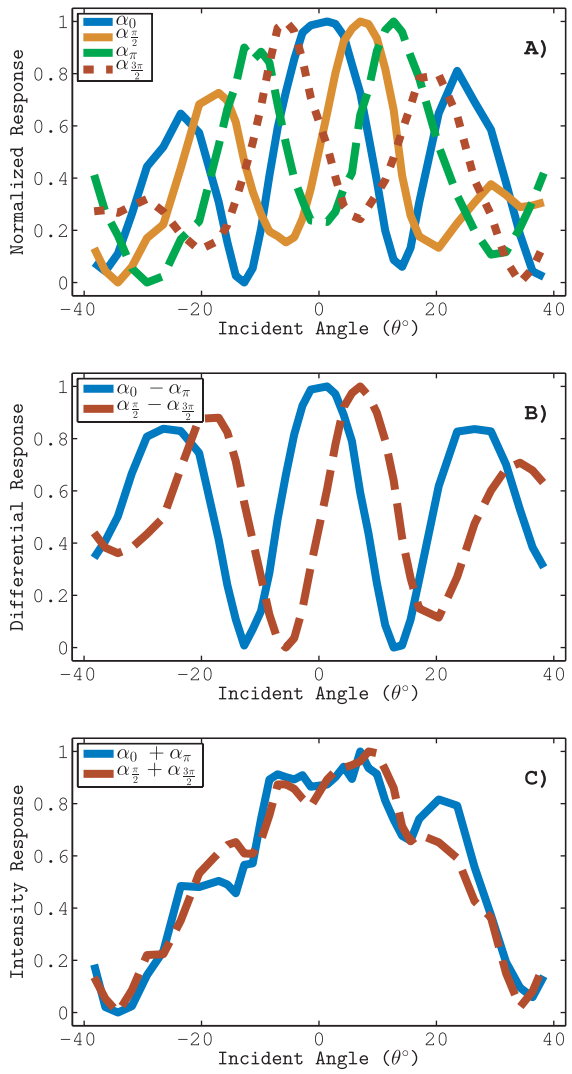

Fig. 10. **A)** Normalized angular response of four ASP subtypes with different analyzer grating offsets. **B)** The difference of complementary ASP subtyptes and **C)** their sum.

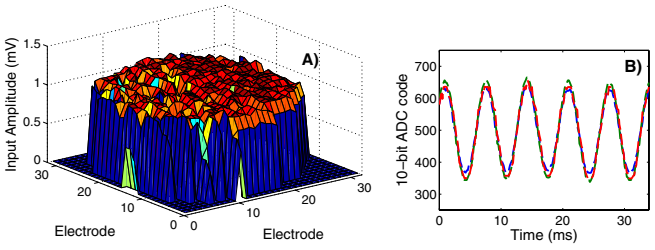

Fig. 11. **A)** Array recording of 1mV sinusoid through a silver chloride wire in aCSF with V_{REF} set to circuit ground. The voltage is the rms value of the input signal. **B)** Digitized output of three adjacent electrodes of data shown in **A**).

B. Measurement Results

Since each front-end amplifier operates open loop, there is a slight gain mismatch between electrodes. To calibrate and demonstrate array functionality, the well was filled with aCSF and stimulated with a 1mV sine wave through a silver chloride wire. Figure 11A shows a three-dimensional map of the input-referred rms voltage recorded by the array. The average gain across the array was 43dB with a standard deviation of 1.8dB. Figure 11B shows a 35ms overlay of three adjacent electrodes from the experiment in Figure 11A.

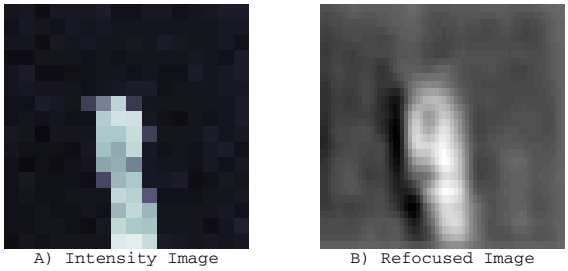

Fig. 12. **A)** Lensless intensity image captured with ASPs of a platinum reference electrode over the sensor array and **B)** computationally refocused image.

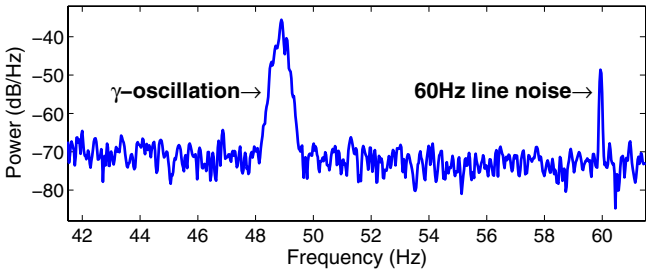

Fig. 13. Power spectrum of a long-lasting gamma oscillation in the olfactory bulb. The gamma oscillation varies in frequency over time creating a broader peak while the 60Hz line noise remains constant resulting in a narrow peak.

To demonstrate the functionality of the optical read-out, a 250μm diameter platinum reference electrode was fixed 200μm above the sensor array. First, an intensity image (sum of complementary ASP subtypes) was captured using an LED illumination source. Then, using synthetic refocus techniques from [20], the image was computationally refocused in software as shown in Figure 12. Refocusing uses the information of the difference between complementary ASP subtypes and then convolves them with scaled, oriented Gabor filters.

To confirm that the sensors could provide sufficiently robust, low noise recording across the full range of biologically relevant signal bands, they were used to record both LFP and spiking activity. The tissue preparation was identical to that used in Section II. A power spectrum of oscillatory activity from a 300μm thick mouse olfactory bulb slice is shown in Figure 13. This data, unfiltered in software, shows an oscillatory peak at the gamma band and a sharp peak at 60Hz due to line noise. The line noise enters the system through the gravity-fed perfusion system and is not inherent to the circuitry. Gamma oscillations arise in the olfactory bulb and change in frequency over time, resulting in a broader peak than the constant frequency line noise. Endogenous spiking activity recorded from the slice is shown in Figure 14. These data were band-pass filtered in MATLAB (200Hz$\leq$f$_{bp}\leq$6kHz) to remove LFP activity.

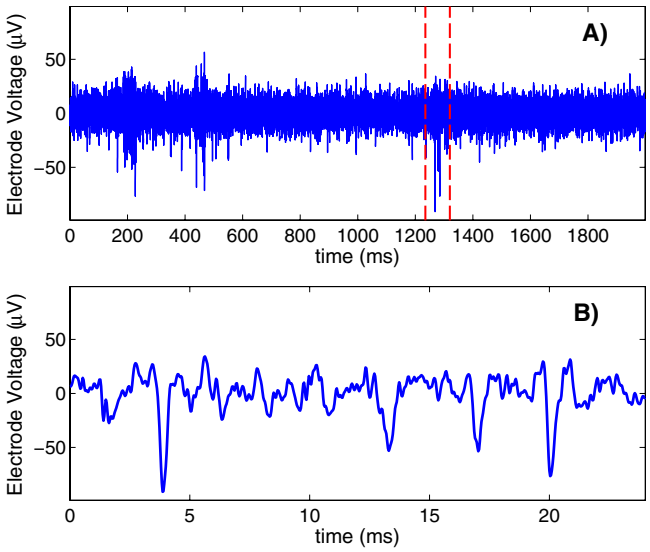

Fig. 14. **A)** A 2000ms recording of extracellular spiking activity recorded from a mouse olfactory bulb slice and a **B)** 25ms subset of **A)**.

V. Conclusion

This paper has presented a highly scalable architecture and demonstration of a CMOS sensor array with metal electrodes and optical sensors. The design was based upon the characteristics of extracellularly recorded neural potentials. Due to a distributed ADC and a compact low-noise front-end amplifier, the system achieves a high-spatial resolution of 50μm without compromising recording area or sampling rate. The system requires simple post-processing to encapsulate the wirebonds and platinize the aluminum electrodes for biocompatibility. The system can perform lensless imaging to localize external electrodes by computationally refocusing information from ASPs. Action potential and LFP recordings from a mouse olfactory bulb slice were also presented. The presented system will enable unique neurophysiological experiments on a chip.

Acknowledgment

The authors would like to thank MOSIS for fabrication support.

References

[1] B. Johnson, S. Peace, T. Cleland, and A. Molnar, "A scalable CMOS sensor array for neuronal recording and imaging," in *Proc. IEEE Sensors*, Nov. 2011, pp. 924–927.

[2] U. Frey, F. Heer, R. Pedron, M. Ballini, J. Mueller, D. Bakkum, S. Hafizovic, F. Faraci, F. Greve, K. Kirstein, and A. Hierlemann, "Switch-matrix-based high density microelectrode array in CMOS technology," *IEEE J. Solid-State Circuits*, vol. 45, no. 2, pp. 467–482, Feb. 2010.

[3] F. Heer, S. Hafizovic, T. Ugniwenko, U. Frey, W. Franks, E. Perriard, J.-C. Perriard, A. Blau, C. Ziegler, and A. Hierlemann, "Single-chip microelectronic system to interface with living cells," *Biosensors Bioelectron.*, vol. 22, no. 11, pp. 2546–2553, May 2007.

[4] E. Boyden, F. Zhang, E. Bamberg, G. Nagel, and K. Deisseroth, "Millisecond-timescale, genetically targeted optical control of neural activity," *Nature Neurosci.*, vol. 8, pp. 1263–1268, Aug. 2005.

[5] A. Wang, P. R. Gill, and A. Molnar, "Fluorescent imaging and localization with angle sensitive pixel arrays in standard CMOS," in *Proc. IEEE Sensors*, Nov. 2010, pp. 1706–1709.

[6] R. Harrison and C. Charles, "A low-power low-noise CMOS amplifier for neural recording applications," *IEEE J. Solid-State Circuits*, vol. 38, no. 6, pp. 958–965, Jun. 2003.

[7] D. H. Gire and N. E. Schoppa, "Long-term enhancement of synchronized oscillations by adrenergic receptor activation in the olfactory bulb," *J. Neurophysiol.*, vol. 99, no. 4, pp. 2021–2025, Feb. 2008.

[8] R. Muller, S. Gambini, and J. Rabaey, "A 0.013 mm^2 5 μW DC-coupled neural signal acquisition IC with 0.5 V supply," *IEEE J. Solid-State Circuits*, vol. 47, no. 1, pp. 232–243, Jan. 2012.

[9] T. P. Zanos, P. J. Mineault, and C. C. Pack, "Removal of spurious correlations between spikes and local field potentials," *J. Neurophysiol.*, vol. 105, no. 1, pp. 474–486, Jan. 2011.

[10] S. V. David, N. Malaval, and S. A. Shamma, "Decoupling action potential bias from cortical local field potentials," *Comput. Intell. Neurosci.*, vol. 2010, pp. 1–12, Nov. 2010.

[11] Z. Yang, Q. Zhao, E. Keefer, and W. Liu, "Noise characterization, modeling, and reduction for in vivo neural recording," in *Advances in Neural Information Processing Systems*. Cambridge, MA, USA: MIT Press, 2010, pp. 2160–2168.

[12] N. Joye, A. Schmid, and Y. Leblebici, "A cell-electrode interface noise model for high-density microelectrode arrays," in *Proc. IEEE 31st Annu. Int. Conf. Eng. Med. Biol. Soc.*, Sep. 2009, pp. 3247–3250.

[13] W. Franks, I. Schenker, P. Schmutz, and A. Hierlemann, "Impedance characterization and modeling of electrodes for biomedical applications," *IEEE Trans. Biomed. Eng.*, vol. 52, no. 7, pp. 1295–1302, Jul. 2005.

[14] U. Frey, U. Egert, D. Jackel, J. Sedivy, M. Ballini, P. Livi, F. Faraci, F. Heer, S. Hafizovic, B. Roscic, and A. Hierlemann, "Depth recording capabilities of planar high-density microelectrode arrays," in *Proc. 4th Int. IEEE/EMBS Conf. Neural Eng.*, May 2009, pp. 207–210.

[15] H. Linden, T. Tetzlaff, T. Potjans, K. Pettersen, S. Grun, M. Diesmann, and G. T. Einevoll, "Modeling the spatial reach of the LFP," *Neuron*, vol. 72, no. 5, pp. 859–872, Dec. 2011.

[16] L. Berdondini, K. Imfeld, A. Maccione, M. Tedesco, S. Neukom, M. Koudelka-Hep, and S. Martinoia, "Active pixel sensor array for high spatio-temporal resolution electrophysiological recordings from single cell to large scale neuronal networks," *Lab Chip*, vol. 9, no. 18, pp. 1–11, 2009.

[17] A. Lambacher, V. Vitzthum, R. Zeitler, M. Eickenscheidt, B. Eversmann, R. Thewes, and P. Fromherz, "Identifying firing mammalian neurons in networks with high-resolution multi-transistor array (MTA)," *Appl. Phys. A. Solids Surf.,* vol. 102, no. 1, pp. 2613–2744, 2011.

[18] J. Aziz, K. Abdelhalim, R. Shulyzki, R. Genov, B. Bardakjian, M. Derchansky, D. Serletis, and P. Carlen, "256-channel neural recording and delta compression microsystem with 3D electrodes," *IEEE J. Solid-State Circuits*, vol. 44, no. 3, pp. 995–1005, Mar. 2009.

[19] A. Wang, P. R. Gill, and A. Molnar, "Angle sensitive pixels in CMOS for lensless 3D imaging," in *Proc. IEEE Custom Integr. Circuits Conf.*, Nov. 2009, pp. 371–374.

[20] A. Wang and A. Molnar, "A light field image sensor in 180 nm CMOS," *IEEE J. Solid-State Circuits*, vol. 47, no. 1, pp. 257–271, Jan. 2012.

[21] M. Dandin, I. D. Jung, M. Piyasena, J. Gallagher, N. Nelson, M. Urdaneta, C. Artis, P. Abshire, and E. Smela, "Post-CMOS packaging methods for integrated biosensors," in *Proc. IEEE Sensors*, Nov. 2009, pp. 795–798.

[22] Y. Liu, E. Smela, N. Nelson, and P. Abshire, "Cell-lab on a chip: A CMOS-based microsystem for culturing and monitoring cells," in *Proc. IEEE 26th Annu. Int. Conf. Eng. Med. Biol. Soc.*, Sep. 2004, pp. 2534–2537.

[23] S. S. A. El-Rahman, "Neuropathology of aluminum toxicity in rats (glutamate and GABA impairment)," *Pharmacol. Res.*, vol. 47, no. 3, pp. 189–194, 2003.

[24] I. S. Steyaert, W. Sansen, and C. Zhongyuan, "A micropower low-noise monolithic instrumentation amplifier for medical purposes," *IEEE J. Solid-State Circuits*, vol. SSC-22, no. 6, pp. 1163–1168, Dec. 1987.

Ben Johnson (S'05) received the B.S. degree in electrical engineering from Oklahoma Christian University, Oklahoma City, OK, USA, in 2007. He is currently pursuing the Ph.D. degree in electrical engineering with Cornell University, Ithaca, NY, USA. His current research interests include low-power mixed-signal circuit design and circuits for neural interfaces.

Shane T. Peace received the B.A. degree in psychology from the University of Louisiana at Monroe, Monroe, LA, USA, in 2004. He is currently pursuing the Ph.D. degree with the Department of Neurobiology and Behavior, Cornell University, Ithaca, NY, USA. His current research interests include mechanisms of gamma band synchronization in the olfactory bulb and methods for combining optical stimulation with multielectrode recordings.

Albert Wang (S'08) received the B.A. degree in chemistry from Harvard University, Cambridge, MA, USA, in 2005, and the Ph.D. degree in electrical engineering from Cornell University, Ithaca, NY, USA, in 2012. He is currently with Apple Inc., Cupertino, CA, USA. His current research interests include analog and mixed-signal circuits and hardware-based signal processing.

Thomas A. Cleland received the B.A. degree in biology from Whitman College, Walla Walla, WA, USA, in 1987, and the Ph.D. degree in biology (neurobiology) from the University of California, San Diego, CA, USA, in 1997. He is currently an Associate Professor with the Psychology Department, Cornell University, Ithaca, NY, USA.

He is a Systems Neuroscientist in the neuronal mechanisms underlying the construction of sensory representations, statistical learning, and memory in the brain, particularly in naturalistic contexts. His research emphasizes neural circuits in the olfactory system, and biomimetic neural algorithms elucidated by Dr. Cleland have been implemented in neuromorphic chips designed for the post-processing of data from arbitrary chemosensor arrays.

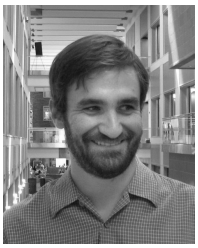

Alyosha Molnar (S'03–M'07) received the B.S. degree (Hons.) in engineering from Swarthmore College, Swarthmore, PA, USA, in 1997, and the M.S. and Ph.D. degrees in electrical engineering from the University of California, Berkeley, CA, USA, in 2003 and 2007, respectively.

From 1998 to 2002, he was with the RF IC Group, Conexant Systems, Inc. (now Skyworks Solutions, Inc.), Newport Beach, CA, USA, where he developed their first generation GSM direct conversion receiver. In August 2007, he joined the Faculty Member of the School of Electrical and Computer Engineering, Cornell University, Ithaca, NY, USA.